https://doi.org/10.15407/ufm.25.02.416

O.L. KASATKIN [1,2,*], O.A. KALENYUK [1,3,], A.O. POKUSINSKYI [4,***], S.I. FUTIMSKY [1,****], and A.P. SHAPOVALOV [1,3,*****]**

[1] G.V. Kurdyumov Institute for Metal Physics of the N.A.S. of Ukraine, 36 Academician Vernadsky Blvd., UA-03142 Kyiv, Ukraine

[2] V.M. Bakul Institute for Superhard Materials of the N.A.S. of Ukraine, 2 Avtozavodska Str., UA-07074 Kyiv, Ukraine

[3] Kyiv Academic University, 36 Academician Vernadsky Blvd., UA-03142 Kyiv, Ukraine

[4] Faculty of Radio Physics, Electronics and Computer Systems, Taras Shevchenko National University of Kyiv, 4[g] Academician Glushkov Ave., UA-03187 Kyiv, Ukraine

* alk@imp.kiev.ua, ** kalenyuk77@gmail.com, *** p.anton.art.fis@ukr.net, **** futimsky@imp.kiev.ua,***** shapovalovap@gmail.com

HIGH-FREQUENCY ELECTRODYNAMICS OF NANOSTRUCTURED MULTIBAND SUPERCONDUCTORS

The effect of artificially created 0*D* and 1*D* structural defects' nanostructure formed by implanted dielectric nanoparticles or irradiation defects on microwave properties of high-T_c superconductor films is analysed based on the phenomenological theory for microwave response of type-II superconductors. The surface resistance is calculated for the Meissner and mixed states for such a kind of nanostructured type-II superconductor film. An emergence of nonlinear response caused by the entrance of microwave-induced vortices in the film interior through its edges is also theoretically explored. The obtained results demonstrate that artificial defect nanostructure inside the superconductor can significantly improve its microwave characteristics in both the Meissner states and the mixed ones and increase the range of the linear microwave response. We also present results of experimental studies on microwave properties of high-temperature superconductor (HTS) films with artificial defect nanostructure formed by heavy-ion irradiation. Noticeable decreases of the surface resistance and enhancement of the linear response range at low temperatures are observed for moderately

Citation: O.L. Kasatkin, O.A. Kalenyuk, A.O. Pokusinskyi, S.I. Futimsky, and A.P. Shapovalov, High-Frequency Electrodynamics of Nanostructured Multiband Superconductors, *Progress in Physics of Metals*, **25**, No. 2: 416–439 (2024)

irradiated HTS $YBa_2Cu_3O_{7-x}$ (YBCO) film exposed to irradiation by 3 MeV Au^{2+} ions at dose 10^{11} cm^{-2}. These results are in agreement with the above-discussed phenomenological theory for microwave response of nanostructured superconductors. A theoretical model concerning the new unusual mechanism of the nonlinear radio-frequency (RF) response in multiband superconductors is also presented. This is a mechanism of nonlinearity based on the possible dissociation of Abrikosov's vortices in multiband superconductors into fractional components under the strong RF current action. We have calculated the RF complex resistivity in two-band superconductors and grounded an emergence of specific peculiarities at critical current density values corresponding to the vortex depinning and dissociation.

Keywords: high-T_c superconductor (HTS), point-like defects, columnar defects, ion irradiation, microwave field, surface impedance, nonlinear response.

1. Introduction

The modern trend in the manufacturing technology of high-temperature superconducting (HTS) materials for the needs of electrical engineering and electronics is connected with the creation of an artificial defect nanostructure inside the superconducting material. Such a nanostructure usually consists of additional nanoscale point or linear structural defects (nanorods) or dielectric inclusions, which serve as strong anchoring points for Abrikosov's vortices and prevent their movement under the Lorentz force action. This type of defect nanostructure can be obtained by implanting dielectric nanoparticles inside the HTS material, as well as by irradiating HTS samples with heavy ions with energies in the range of several MeV (to create 0*D* structural defects) or several GeV (to create 1*D* extended columnar defects — radiation tracks with nanoscale cross-section). These additional nanoscale structural defects generally are places of strong pinning of vortices, which increase the value of the critical current [1–11]. On the other hand, as follows from some experimental works, the implantation of dielectric nanoparticles, as well as the formation of point radiation defects in the matrix of the HTS film can significantly improve its microwave characteristics. For example, implanted dielectric nanoparticles and nanorods of different nature and content, as well as radiation nanoscale defects can significantly reduce the surface resistance, $R_s(T, \omega)$, in the Meissner state [12, 13] and the contribution of forced oscillations of Abrikosov's vortices and related microwave energy losses to the surface resistance in the mixed state of superconductor, $R_{s,v}(B, T, \omega)$ [14–16].

This paper presents the results of a theoretical study of the influence of point and extended linear defects on the microwave surface impedance in the Meissner and mixed states of superconductors with one and two conducting electron bands. As shown, the artificial defect nanostructure contributes to the reduction of the surface resistance of superconductors in the microwave range and increases the linear response range. The results of an experimental study of the microwave surface impedance per-

formed on the HTS films $YBa_2Cu_3O_{7-x}$ (YBCO) irradiated with high-energy Au^{2+} ions (3 MeV) are presented, which confirms the positive role of nanoscale radiation defects, that arose as a result of ion irradiation, in the reduction of the surface resistance for investigated films and increasing their range of linearity. A theoretical model of vortex dissociation into fractional components under the strong radio frequency (RF) field action and related specific RF nonlinearity effects in two-band superconductors in the mixed states is proposed.

2. Effect of Nanostructural Defects on $R_s(T, \omega)$ in the Meissner State of Superconductor

In the framework of the two-fluid model for the superconducting state the complex microwave surface impedance and conductivity of a fairly thick superconducting film $d > 2\lambda$ (d is the film thickness, λ is the London penetration depth) being in the Meissner state, are described by the well-known relations [12, 16–18]:

$$Z_s(\omega, T) = R_s(\omega, T) + iX_s(\omega, T) = \left(\frac{i\omega\mu_0}{\sigma_1(\omega, T) - i\sigma_2(\omega, T)} \right)^{1/2}. \quad (1)$$

For temperatures slightly lower than T_c, when $\sigma_1 << \sigma_2$,

$$R_s(T, \omega) = \frac{1}{2}\mu_0^2\omega^2\lambda^3(T)\sigma_1(T, \omega), \quad X_s(T, \omega) = \mu_0\omega\lambda(T), \quad (2)$$

$$\sigma_1(T, \omega) = \frac{e^2}{m^*} n_n(T) \frac{\tau(T)}{1 + (\omega\tau(T))^2}, \quad \sigma_2(T, \omega) = \frac{1}{\mu_0\omega\lambda^2(T)} = \frac{e^2}{m^*\omega} n_s(T). \quad (3)$$

Here, $\sigma(T,\omega) = \sigma_1(T,\omega) - i\sigma_2(T,\omega)$ is the complex microwave conductivity, $\sigma_1(T,\omega)$ and $\sigma_2(T,\omega)$ are its real and imaginary parts, respectively, determined by Eq. (3); $n_n(T)$ and $n_s(T)$ are the concentrations of normal and superconducting electrons, respectively: $n_n(T) + n_s(T) = n_0$ (n_0 is the total density of conduction electrons); $\tau(T)$ is the pulse relaxation time for normal electrons. Within the framework of the phenomenological theory, we can assume that $\tau^{-1}(T) = \tau_0^{-1} + \tau_i^{-1} + \tau_{e\text{-}ph}^{-1}(T)$, where τ_0, τ_i, $\tau_{e\text{-}ph}(T)$ are relaxation times corresponding to electron scattering on natural defects in the initial film, on implanted dielectric nanoparticles or radiation-induced structural defects, and on thermally excited phonons, respectively. The addition of nanoscale defects increases the overall scattering rate $\tau^{-1}(T)$, and according to Eqs. (2) and (3), this should lead to a decrease in $\sigma_1(T, \omega, n_i)$ and $R_s(n_i, \omega, T)$, respectively. On the other hand, there is an opposing factor — an increase in the London penetration depth $\lambda(T)$ with increasing disorder, which is characterized by a decrease in the mean free path length, $l \approx v_F\tau$ of normal electrons (here, v_F is the Fermi velocity). For d-wave superconductors, such as HTS rare-earth barium copper oxide (REBCO) cu-

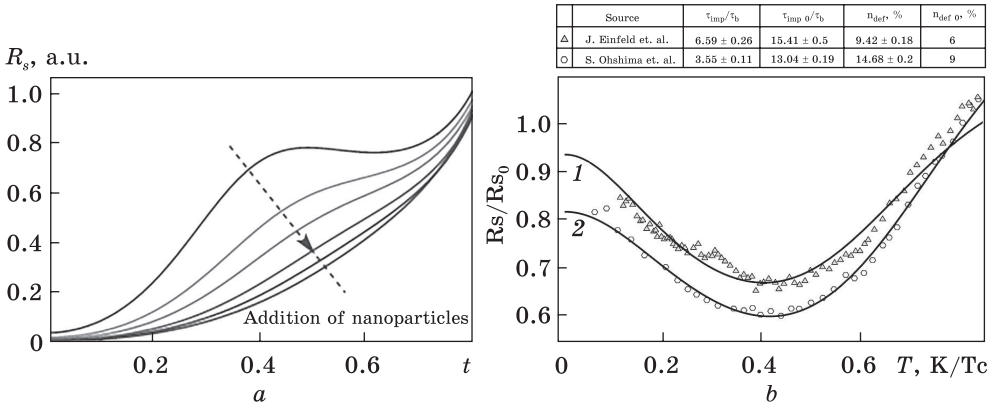

Fig. 1. Theoretical effect of adding dielectric nanoparticles or nanosized radiation defects on the surface resistance $R_s(T)$ at different reduced temperatures $t = T/T_c$ (*a*). Experimental data for the ratio of surface resistances of the YBCO film with an artificial defective nanostructure and the primary YBCO film, adopted from experiments (*b*) [12, 13]. The solid curves demonstrate the possible fitting of these data using this theory (Eqs. (2), (3), (6)). The corresponding fit parameters are listed in the table inside this figure; $n_{def}(\%) = n_{def}/n_0$ (%) [16]

prates, this effect was considered in works [19, 20] and the following extrapolation formula for $\lambda(T)$ was obtained

$$\lambda(T) = \tilde{\lambda}(0) + \alpha \frac{T^2}{T + T^*}, \tag{4}$$

where T^* is the characteristic temperature of the transition from a quadratic dependence at low temperatures to a linear one at high temperatures in a 'dirty' d-wave superconductor with nodal directions in the electronic spectrum $E(p)$: $k_B T^* \cong 0.83\sqrt{\Gamma\Delta(0)}$, where $\Gamma = n_i n_0/\pi N(0)$ is the scattering rate parameter, $\Delta(0)$ is the amplitude of the anisotropic d-wave gap in the electronic spectrum at zero temperature, and $N(0)$ is the density of electronic states at the Fermi level. It can be estimated that $T^* \cong 0.01T_c$ is a typical value for high-quality HTS material YBCO. From the considerations given in Refs. [19, 20], which seems to be relevant for the HTS REBCO films, it follows that

$$\tilde{\lambda}(0)/\lambda(0) = 1 + 0.95k_B T^*/\Delta(0) = 1 + 0.44T^*/T_c \equiv 1 + 0.44t^*, \tag{5}$$

$$\lambda(t) \cong \lambda(0)\left[1 + 0.44t^* + 0.32\frac{t^2}{t + t^*}\right](1 - t^2)^{-1/2}, \tag{6}$$

where $t = T/T_c$ is the reduced temperature. Using Eqs. (1), (2), (6), it is possible to investigate the reduction of $R_s(T)$ values due to the addition of nanoscale structural defects (for example, implantation of dielectric nanoparticles or radiation defects) in the inner part of the superconduc-

ting film. We calculated typical dependences of $R_s(T)$ for HTS films with different values of ni, using the corresponding values for other parameters taken from relevant experimental works (see, for example, [12, 13]). The effect of disorder on the $R_s(T)$-dependences caused by the implantation of nanoscale structural defects is demonstrated in Fig. 1. The addition of nanoscale structural defects with a concentration ni inside the superconductor leads to a decrease in the relaxation rate $\tau^{-1}(T)$, and, according to Eqs. (2) and (3), to a decrease in $\sigma_1(T, \omega, n_i)$ and $R_s(n_i, \omega, T)$, respectively, too. This reduction of $R_s(n_i, \omega, T)$ is most pronounced at moderate temperatures $T \cong 0.5T_c$, as it follows from our numerical results presented in Fig. 1, and is in good agreement with experimental data [12, 13]. An increase in the concentration of nanoscale structural defects n_i also leads to a significant increase in the penetration depth, λ, as follows from Eqs. (4)–(6). The latter manifests itself mainly at low temperatures, as shown in Fig. 1. These results are consistent with experimental data obtained on HTS REBCO films [12–14].

3. Vortex Oscillations and Related Contribution to $R_s(B, T, \omega)$ in the Mixed State of Superconductor

In the mixed state of the superconductor, a certain contribution to the surface impedance in the microwave range is given by forced viscous oscillations of Abrikosov's vortices. At not very high values of the permanent magnetic induction, B, the total surface resistance $R_s(n_i, B, \omega, T)$ can be considered as consisting of two contributions: $R_s(n_i, B, \omega, T) = R_{s,e}(n_i, \omega, T) + R_{s,v}(n_i, B, \omega, T)$, where $R_{s,e}$ is the contribution of quasiparticles determined by Eq. (2), while $R_{s,v}$ corresponds to the contribution of oscillating vortices. In works [15–17], we obtained analytical expressions for the vortex contribution $R_{s,v}$ to the surface resistance of HTS material with various types of nanosized defects, namely point and extended linear (columnar) defects, which are schematically shown in Figs. 2 and 3, respectively. In these calculations, we used the single-vortex approximation and neglected collective effects in the vortex ensemble. In the case of vortex pinning caused by columnar defects, the main contribution to $R_{s,v}$ at moderate temperatures $T < T_c$ is due to the high-frequency dynamics of thermally excited vortex kinks, as shown in Fig. 3. These vortex kinks connect two parts of the entire vortex line, located on two adjacent columnar defects, and can move viscously along the axis of these defects (z-axis in Fig. 3) under the action of the Lorentz force. When the magnetic field is inclined to the axis of columnar defects, the number of kinks and their equilibrium concentration inside the film are controlled by the angle of inclination (see Fig. 4). Both cases are discussed below.

In the case of point pinning centres, the oscillations of vortices under the action of a high-frequency current are broken down into oscillations of

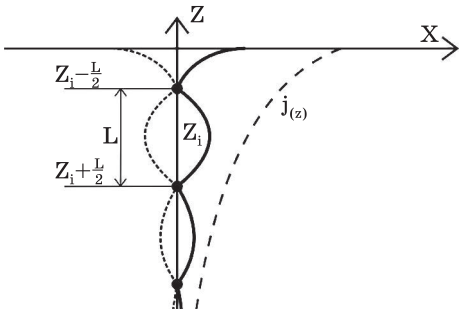

Fig. 2. High-frequency oscillations of an elastic vortex string anchored by point pinning centres [15]

individual segments of the vortex line by the adjacent centres of its pinning. Vortex segments between adjacent pinning point centres located along the entire vortex line oscillate under the action of the high-frequency Lorentz force, which is induced by the high-frequency current. These vortex segments behave as nearly independent overdamped oscillators. The elastic deformation energy of these segments, bent under the Lorentz force, plays the role of potential energy for these oscillators. This potential energy can be easily calculated from the equation that defines the displacement of the vortex segment $s(z)$ from the equilibrium position under the action of the Lorentz force, supplemented by the appropriate boundary condition corresponding to the fixed ends of the vortex segment [22]:

$$P\frac{d^2s}{dz^2} + \phi_0 j(z) = 0. \tag{7}$$

The boundary conditions for Eq. (7) correspond to the rigid fixation of the ends of the vortex line in the positions of the point pinning centres, separated from each other by a distance L, *i.e.*, $s(0) = s(L) = 0$, as schematically shown in Fig. 2. In Eq. (7), $j(z)$ is the local current density; P is the coefficient of elasticity of the vortex line. The bending of the vortex segment under the action of the Lorentz force increases its energy of elastic deformation. The latter plays the role of a pinning potential well, U_p, for oscillations of the vortex segments, fixed by the neighbouring point pinning centres (see Fig. 2). Calculations of high-frequency losses and the associated surface resistance due to high-frequency vortex oscillations within the Gittelman–Rosenblum model [26] lead to the following result for the considered case of oscillating vortex segments [15, 16]:

$$R_{s,v} \propto \frac{B}{B_{c2}}\rho_n \frac{\omega^2}{\omega_p^2 + \omega^2}, \quad \omega_p = \frac{12P}{\eta L}. \tag{8}$$

In Eq. (8), ρn is the specific resistance in the normal state ($T > T_c$), ω_p is the so-called 'pinning frequency' [21], and is the viscosity coefficient for vortex motion. An increase in the concentration of point structural defects leads, in turn, to a decrease in the length of the vortex segments L and a corresponding increase in ω_p, which leads to a decrease in the surface resistance according to the formula (8).

For the case when the main type of vortex pinning centres is columnar defects, we believe that the microwave losses associated with vortex oscil-

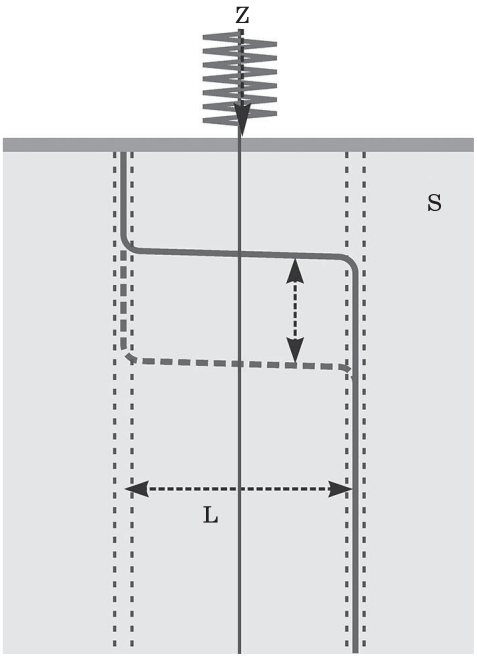

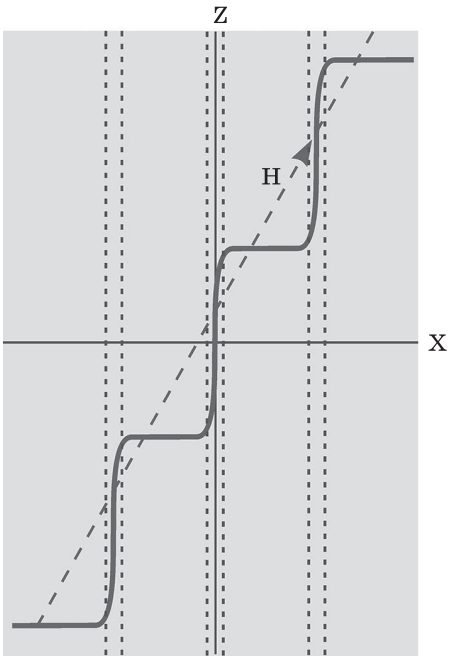

Fig. 3. The RF oscillations of vortex kinks in a superconductor with columnar defects [16]

Fig. 4. Formation of vortex kinks in a tilted magnetic field — vortex stairs [16]

lations in the high-frequency field are caused by viscous vibrations of vortex kinks that connect parts of the vortex line anchored to adjacent columnar defects as well as pinned parts of the vortex line that are in potential pinning pits formed by columnar defects. This is shown schematically in Fig. 3. Next, we consider a step vortex structure that arises in an applied magnetic field tilted by an angle θ relative to the axis of the columnar defects, and consists of vortex parts anchored by the columnar defects and vortex kinks connecting these anchored vortex parts [1, 3, 4, 16], as schematically shown in Fig. 4. Further, we assume that the parts of the vortex line anchored on the columnar defects settle in the potential pinning pit $U_p(u)$, where u is the displacement of the anchored part of the vortex line from the axis of the columnar defect (z-axis), and the vortex kinks, are assumed to be parallel to the two-dimensional superconducting layers in a layered superconductor (*e.g.*, Cu–O layers in HTS REBCO), can oscillate along the columnar defect axis under the action of the Lorentz force, being in the potential well $U_\perp(s)$ created by the internal pinning mechanism in layered structures (the so-called 'intrinsic pinning mechanism' [23, 27]), or point defects, which usually also exist in layered superconductors with columnar defects and can immobilize vortex kinks (here, s is the vortex kink displacement along the z-axis under the Lorentz force

action; see Fig. 3). For small displacements u ($u << r_p$), the pinning potential can be approximated as follows

$$U_p(u) \simeq -U_{p0} + \frac{\alpha_L}{2} u^2, \quad \alpha_L = \frac{2U_{p0}}{r_p^2}, \tag{9}$$

where α_L is the so-called Labusch parameter [23, 27], which characterizes the stiffness of the potential pinning pit near its bottom. Similarly, we choose the pinning potential for vortex kinks, $U_\perp(s)$, in the form:

$$U_\perp(z) = -U_{\perp,0} + \frac{\alpha_{L,\perp}}{2}(z - z_i)^2, \ \ |z - z_i| < \xi_c. \tag{10}$$

The dynamic equation for small high-frequency oscillations of a vortex kink, located in the potential tip of the vortex's internal ('intrinsic') pinning, under the RF Lorentz force action $F_L = \phi_0 j(z,t) = \phi_0 j_0 e^{z/\lambda + i\omega t}$ ($z < 0$) can be written as [16]

$$\begin{gathered} \eta_{\phi,\perp} \frac{\partial}{\partial t} s(z_i,t) = -\frac{\partial U_\perp}{\partial s} + F_L(z_i,t), \ \ s(z_i,t) = z(t) - z_i, \\ i\omega\eta_{\phi,\perp} s(z_i) = -\alpha_{L,\perp} s(z_i) + \phi_0 j(z_i) \sin\varphi_i, \end{gathered} \tag{11}$$

where $s(z_i,t) = s_\omega e^{z_i/\lambda + i\omega t} \propto j(z_i,t)$ is the displacement of the kink from its equilibrium position zi at one of the minima of the pinning potential $U_\perp(s)$; $\eta_{\phi,\perp}$ is the viscosity coefficient for the vortex kink motion along the z-axis (per unit kink length); φ_i is the azimuthal angle between the i-th kink and the current direction in the plane of $2D$ superconducting layers (ab plane). Similarly, the dynamic equation for small high-frequency oscillations of a vortex segment fixed by a columnar defect (for example, in the interval $z_i < z < z_{i+1}$) can be written as follows [16]:

$$\begin{gathered} \eta_{\phi,\parallel} \frac{\partial}{\partial t} u(z,t) = P \frac{\partial^2 u}{\partial z^2} - \frac{\partial U_p}{\partial u} + F_L(z,t), \ \ z_i < z < z_{i+1}, \\ i\omega\eta_{\phi,\parallel} u(z) = P \frac{\partial^2 u}{\partial z^2} - \alpha_L u(z) + \phi_0 j(z), \end{gathered} \tag{12}$$

where $u(z,t) = u_\omega e^{z/\lambda + i\omega t} \propto j(z,t)$ is the vortex segment displacement from the columnar defect axis under the RF Lorentz force influence; $\eta_{\phi,\parallel}$ is the viscosity coefficient for the vortex segment motion parallel to the (x,y) plane (per unit length). From Eqs. (11) and (12) for the complex amplitudes of vortex displacements — s_ω and u_ω, respectively, we obtain

$$s(z_i,t) = \frac{\phi_0 j_0 e^{z_i/\lambda + i\omega t} \sin\varphi_i}{\alpha_L + i\omega\eta_{\phi,\perp}} \ \ (z_i < 0), \tag{13}$$

$$u(z,t) = \frac{\phi_0 j_0 e^{z/\lambda + i\omega t}}{\alpha_L(1 - L_p^2/\lambda^2) + i\omega\eta_{\phi,\parallel}} \ \ (z < 0). \tag{14}$$

In Eq. (14), $L_p = \sqrt{P/\alpha_L}$ is the characteristic scale of the vortex line bending [15, 16].

Following the approach of the Gittelman–Rosenblum model [26], we extend this model to the case of an elastic vortex line in a superconductor with a system of parallel equidistant columnar defects oriented perpendicularly to the sample surface. We assume that the vortices are created by a magnetic field tilted to the defect axis (z-axis). Therefore, in this case, the vortex line in equilibrium has the shape of a ladder (schematically shown in Fig. 4) and oscillates under the action of a non-uniformly distributed RF Lorentz force: $F_L = j(z,t)\phi_0$. By analogy with [26], we can write the equation for the dissipated high-frequency power, W_{dis}, as follows:

$$W_{dis} = \frac{n_\phi}{2}\int_{-\infty}^{0} \mathrm{Re}\left[\mathbf{F}_L^*(z,t)\mathbf{v}_\phi(z,t)\right]dz = \frac{1}{2}R_s I^2, \quad I = \int_{-\infty}^{0} j(z)dz = j_0\lambda. \tag{15}$$

In Eq. (9), the local vortex velocity is given by (see Fig. 1)

$$\mathbf{v}_\phi(z,t) = \frac{\partial \mathbf{u}(z,t)}{\partial t}, \ z_i < z < z_{i+1}; \ \mathbf{v}_\phi(z_i,t) = \frac{\partial \mathbf{s}(z_i,t)}{\partial t}, \ z = z_i. \tag{16}$$

n_ϕ is the two-dimensional density of vortices on the sample surface: $n_\phi\phi_0 = B_\perp = B\cos\theta$ (B is the magnetic induction in the mixed state of the superconductor); I is the amplitude of the high-frequency Meissner current in the surface shielding layer (sheet current). For the step structure of the vortex line anchored by columnar defects, we can evaluate the integral in the first of Eq. (15) as the sum of two terms, corresponding to the oscillations of the vortex segments anchored on the columnar defects and the vortex kinks, connecting these segments on neighbouring columnar defects, as schematically shown in Figs 3 and 4,

$$W_{dis} = \frac{n_\phi}{2}\int_{-\infty}^{0} \mathrm{Re}\left[F_L^*(z,t)\frac{\partial u(z,t)}{\partial t}\right]dz + \\ + \frac{1}{2}\sum_i \mathrm{Re}\left[F_L^*(z_i,t)\frac{\partial s(z_i,t)}{\partial t}\right]n_k(z_i)L\sin^2\varphi_i = \frac{1}{2}\left(R_{s,v}^{(1)} + R_{s,v}^{(2)}\right)I^2. \tag{17}$$

Consistent calculations based on this approach, carried out by the authors in Ref. [16], allowed us to obtain expressions for the surface resistance in the form

$$R_{s,v}^{(1)} = \frac{\rho_{f,\parallel}(B)}{2\lambda}\frac{\omega^2\cos\theta}{\omega_{p,\parallel}^2 + \omega^2}, \ \rho_{f,\parallel}(B) = \frac{\rho_{n,\parallel}B}{B_{c2,\perp}}, \ \omega_{p,\parallel} = \frac{\alpha_{L,\parallel}(1 - L_p^2/\lambda^2)}{\eta_{\phi,\parallel}}. \tag{18}$$

Here, $\rho_{f,\parallel}(B)$ is the flux-flow resistivity in the (x,y)-plane, *i.e.*, parallel to the sample surface (as well as to two-dimensional superconducting layers in layered materials such as REBCO), $\rho_{n,\parallel}$ is the resistivity of the normal state in this direction, and $B_{c2,\perp}$ is the upper critical field for ori-

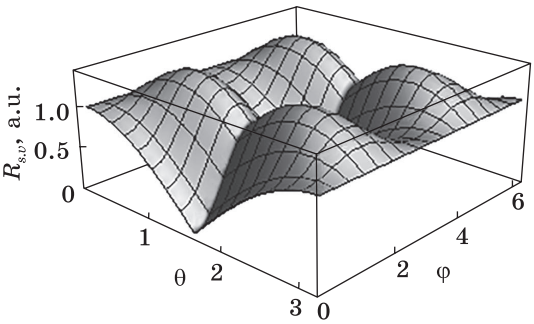

Fig. 5. Field-induced anisotropy of the surface resistance (20) in an isotropic superconductor with columnar defects [17]

entation along the z-axis (*i.e.*, perpendicularly to the planes of two-dimensional layers); $\omega_{p,\|}$ is the so-called pinning frequency [21] for oscillations of vortex segments in potential pinning tips $U_p(u)$ of columnar defects. Then,

$$R_{s,v}^{(2)} = \frac{\rho_{f,\perp}(B)}{2\lambda}\frac{\omega^2\Theta(\theta-\theta_c)\sin\theta\sin^2\phi}{\omega_{p,\perp}^2+\omega^2},\ \rho_{f,\perp}(B)=\frac{\rho_{n,\perp}B}{B_{c2,\|}},\ \omega_{p,\perp}=\frac{\alpha_{L,\perp}}{\eta_{\phi,\perp}}. \quad (19)$$

Here, $\rho_{f,\perp}(B)$ is the flux-flow resistivity in the z-direction, *i.e.*, perpendicularly to the two-dimensional superconducting layers, $\rho_{n,\perp}$ is the resistivity of the normal state in this direction, and $B_{c2,\|}$ is the upper critical field for the magnetic field orientation parallel to the plane of two-dimensional layers; $\omega_{p,\perp}$ is the pinning frequency for vortex kink oscillations in the potential tips of the intrinsic pinning $U_{2D}(s)$; $\Theta(\theta-\theta_c)$ is a step function; θ_c is the so-called 'locking angle' [27], which defines a small range of angles $\theta < \theta_c$ when vortices are completely anchored by columnar defects and no kinks appear in the equilibrium state; φ is the azimuthal angle between the current and kink directions (all kinks should now be located in the (H,z)-plane).

The total contribution of vortices to the surface resistance $R_{s,v} = R_{s,v}^{(1)} + R_{s,v}^{(2)}$. In the isotropic case, when $\rho_{f,\perp}(B) = \rho_{f,\|}(B) = \rho_f(B)$, $\omega_{p,\perp} = \omega_{p,\|} = \omega_p$ it can be written as follows

$$R_{s,v} = \frac{\rho_f(B)}{2\lambda}\frac{\omega^2}{\omega_p^2+\omega^2}(\cos\theta+\sin\theta\sin^2\varphi). \quad (20)$$

The field-induced anisotropy given by Eq. (20) is demonstrated in Fig. 5. This result indicates the fundamental possibility of tuning the microwave surface resistance by changing the magnitude and orientation of the applied magnetic field.

4. Effect of Defect Nanostructure on the Linearity of Microwave Response

The problem of nonlinear microwave response of HTS films is very important for applications and this is one of the most fundamental problems of microwave superconductivity. There are various sources of nonlinearity at microwave frequencies in HTS films, which have been intensively discussed

in several papers (see, *e.g.*, [28–32]). For thin-film microwave devices, characterized by a high concentration of high-frequency current at the edges of the film, such as microstrip or coplanar microwave resonators and transmission lines made of high-quality HTS films free from high-angle grain boundaries and other types of intrinsic weak connections, the main source of nonlinearity is associated with the creation of microwave-induced vortices and their further propagation inside the HTS film under the action of a high-frequency current with an amplitude, which exceeds a certain threshold value of the current density, j_v, which determines the range of linear response [30–32].

Here, we demonstrate that the implantation of additional strong vortex pinning sites in the form of nanoscale point or extended linear defects can noticeably increase the j_v threshold value, thereby increasing the linear response range. We consider the case of nonlinearity caused by the penetration of microwave-induced Abrikosov vortices into a bulk superconducting sample through its flat surface. These induced vortices move inside the superconductor under the influence of the RF Meissner current $j(x, t) = j_0 e^{-x/\lambda}\sin(\omega t)$. The appropriate equation of vortex dynamics exerted to the RF Lorentz force $F_{L,rf}(x,t)$ action caused by the high-frequency current $j(x, t)$, with account for vortex attraction to its image on the outer side of the sample's flat surface and viscous friction of vortices, has the form [32]

$$\eta\dot{x} = \phi_0 j_0 e^{-x/\lambda}\sin(\omega t) - \frac{\phi_0^2}{2\pi\mu_0\lambda^3} K_1\left(\frac{2\sqrt{x^2+\xi_s^2}}{\lambda}\right). \qquad (21)$$

Here, $K_1(z)$ is the McDonald function of the 1-st order, and ξ_s is the local coherence length on the surface of the sample. The last term in the right-hand side of Eq. (21) describes the attraction of vortex line, which is parallel to the sample surface, to its anti-vortex image on the opposite side of the sample surface and determines the Bean–Livingstone barrier for the entrance of vortices inside the superconductor: $F_b(x) = -dU_{int}(2x)/dx$, where $U_{int}(2x)$ is the interaction energy of a vortex located at a distance x from the surface inside the superconductor, with its image of the opposite sign, located at the point $-x$ outside the sample. From Eq. (21), it follows that additional vortices induced by the microwave current can penetrate inside the superconductor through its surface when the Lorentz force at the sample's surface ($x = 0$) overcomes the restoring force caused by the surface barrier, $F_b(x = 0)$, *i.e.*, when the amplitude of the RF current on the surface, j_0, will exceed some threshold value, j_v. From Eq. (21), it follows that [32]

$$j_v = \frac{\phi_0}{4\pi\mu_0\lambda^2\xi_s} \approx 0.71\frac{B_c}{\mu_0\lambda}, \qquad (22)$$

where B_c is the thermodynamic critical field of the superconductor. An

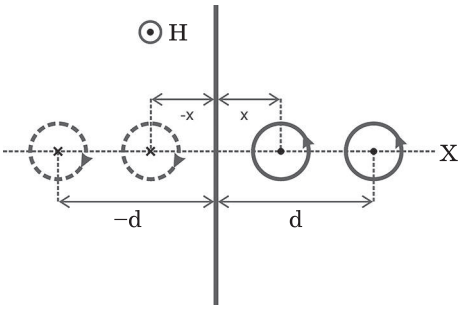

Fig. 6. The columnar defect with a trapped vortex on it inside the superconductor, oriented parallel to the sample surface at a distance d from it, and a new vortex created by the RF field at the distance x from the surface, as well as the images of these vortices placed on the opposite side of the sample surface [16]

addition of vortex-strong pinning sites can significantly increase the effective surface barrier for vortex penetration and prevent the entrance of new vortices induced by the microwave field, thus increasing the magnitude of the threshold current j_v. The latter, in turn, determines the range of linearity of the microwave response. This statement can be qualitatively argued based on the simplified model schematically depicted in Fig. 6. At high amplitudes of the microwave current density $j_0 > j_v$, microwave-induced vortices will penetrate the superconductor through the surface and be fixed on the nearest linear defects, which will prevent their further propagation into the depth of the material. At the same time, vortices that penetrated earlier during the transition process and were captured by strong pinning centres near the surface (at some distance $d < \lambda$, as schematically shown in Fig. 6), will increase the effective surface barrier. Their role can be taken into account by including two additional terms in Eq. (15):

$$\eta\dot{x} = \phi_0 j_0 e^{-x/\lambda} \sin(\omega t) - \frac{\phi_0^2}{2\pi\mu_0\lambda^3} K_1\left(\frac{2\sqrt{x^2+\xi_s^2}}{\lambda}\right) -$$

$$-\frac{\phi_0^2}{2\pi\mu_0\lambda^3} K_1\left(\frac{2\sqrt{(x-d)^2+\xi_s^2}}{\lambda}\right) - \frac{\phi_0^2}{2\pi\mu_0\lambda^3} K_1\left(\frac{2\sqrt{(x+d)^2+\xi_s^2}}{\lambda}\right). \qquad (23)$$

The last two terms in the right-hand side of Eq. (23) describe the interaction of the additional vortex entering the sample through the surface with the vortex previously captured on the linear defect at a distance d from the surface, as well as with its image of the opposite sign located at the point $-d$ outside the surface. As follows from Eq. (23), the threshold value of the current density j_v defined earlier in Eq. (22) now takes the form

$$j_v = \frac{\phi_0}{4\pi\mu_0\lambda^2\xi_s} + \frac{\phi_0}{\pi\mu_0\lambda^2\sqrt{d^2+\xi_s^2}}. \qquad (24)$$

The last term in the right-hand side of Eq. (24) describes the increase in the linearity threshold due to implanted strong vortex pinning sites, as discussed above and illustrated here using this simplified model with an extended linear defect acting as a vortex trap. A significant increase in

the threshold value of the linearity threshold, j_v, due to the implantation of nanosize strong pinning sites for vortices in the inner part of HTS films (YBCO) was observed experimentally in works [33, 34].

5. Microwave Response of YBCO Films Irradiated with Heavy Ions

Experimentally, the effect of defect nanostructure on the high-frequency electrodynamics of superconducting materials was studied on HTS films irradiated with heavy, high-energy ions [35]. We explored the effect of irradiation of YBCO pulse-laser-deposited thin films by Au^{2+} ions with energy of 3 MeV at different irradiation doses on the microwave surface impedance $Z_s = R_s + iX_s$, both in linear and nonlinear modes. As follows from the structural studies carried out in [36, 37], the main type of radiation defects, in this case, are point structural defects with a size of several nanometres, and the depth of their penetration into the YBCO film is on the order of 100 nm from the film surface. It was found that such ion irradiation of YBCO films does not affect the measured microwave characteristics of these films at low doses of irradiation (~10^{10} cm^{-2}), while at moderate doses of irradiation (~10^{11} cm^{-2}), it significantly improves the electrodynamic characteristics of the film at microwave frequencies by reducing its surface resistance $R_s(T)$ and improving the linearity of the microwave response at low temperatures. These effects are explained based on phenomenological theory [15–17], described in the previous sections of this article.

The explored thin films of the high-temperature superconductor YBCO with a thickness of 200 nm, a critical temperature $T_s = 90$ K, and a width of the superconducting transition <1 K were obtained by laser deposition on polished sapphire substrates with a thickness of 0.5 mm. The produced YBCO films were irradiated with Au^{2+} ions with an energy of 3 MeV accelerated by a Van de Graaf tandem accelerator (Ion Beam Centre HZDR) at room temperature in a vacuum of 10^{-5} Pa. The angle of incidence of the ions was chosen normal to the surface of the film. The ion dose (Φ) was controlled by adjusting the ion fluency and the sample exposure time (<10 s). The expected range of ion penetration depths in the YBCO film is 200–600 nm from the film surface [37]. The details of the performed experiments are as follows [35]: at the first stage, the double-sided YBCO film on the sapphire substrate was divided into several parts of 10×10 mm^2 size. After that, these parts of the film were irradiated with Au^{2+} ions with energy of 3 MeV at three irradiation doses: $\Phi = 10^{10}$ cm^{-2}, 10^{11} cm^{-2}, and 10^{12} cm^{-2}. Subsequently, identical meanders for microstrip resonators were made from these irradiated areas of the film, as well as from the original film, by the method of standard photolithography with etching in a phosphoric acid solution. As a result, YBCO microstrip resonators with an irradiated meander and a non-irradiated substrate were obtained.

The microwave studies of the investigated films were carried out using standard two-port microwave measurements of the amplitude-frequency characteristics (AFC) — the transmission coefficient $S_{21}(f)$ as a function of the frequency f. Such measurements for these resonators were carried out using a Keysight P9375A vector network analyser. It provided operation in the frequency range from 300 kHz to 26 GHz and in the power range of $1 \cdot 10^{-4} - 0.1$ W with a power amplifier. Parameter $S_{21}(f)$ can be determined using two-port simultaneous measurements when the measured transmitted microwave power from port 2 is compared with the input signal passed through the resonator at port 1. Thus, the amplitude-frequency response (AFC) was obtained, from which the value of the resonant frequency, $F(T, I_{RF})$, and quality factor, $Q(T, I_{RF})$, was calculated depending on the temperature T and the amplitude of the microwave current I_{RF} in the film. For sample $S1$ at the temperature of 5 K and at the minimal microwave power, the following values of the quality factor and resonant frequency were obtained: $Q = 144750$ and $F = 1.14$ GHz.

The obtained experimental results regarding the values of the Q factor and the resonance frequency F make it possible to calculate the surface resistance R_s, which is the real part of the surface impedance Z_s ($Z_s = R_s + iX_s$), and the changes in its imaginary part ΔX_s caused by the change in temperature T and/or the amplitude of the microwave current I_{RF} in the resonator. This calculation can be performed using the known relations [21]:

$$R_s(T, I_{RF}) = \Gamma \frac{1}{Q(T, I_{RF})}, \quad \Delta X_s(T, I_{RF}) = 2\Gamma \frac{F_0 - F(T, I_{RF})}{F_0}, \qquad (25)$$

where F_0, F, and Q are the initial and changed (due to changes in temperature and/or microwave current) values of the frequency and Q-factor of the resonator, respectively; Γ is the so-called geometric factor of the resonator, which depends on the geometry of the microwave currents in the resonator and can be calculated by numerical methods.

Obtained results for dependences of the impedance on a temperature and microwave current IRF, presented in Figs. 7 and 8, for pristine and irradiated by 3 MeV Au^{2+} ions YBCO films from which these resonators were made. The temperature dependences of the surface impedance (both real and imaginary parts) for these films are shown in Fig. 7. There are three curves for both the surface resistance, $R_s(T)$ and the change in surface reactance, $\Delta X_s(T)$, corresponding to different irradiation doses: S0 is the unirradiated pristine YBCO film, while $S1$ and $S2$ correspond to irradiated films with different radiation doses: $S1$ — 10^{11} cm^{-2}; $S2$ — 10^{12} cm^{-2}. As for the YBCO film irradiated with the lowest dose — 10^{10} cm^{-2}, for this film, the dependences $R_s(T)$ and $\Delta X_s(T)$ turned out to be the same as for the pristine non-irradiated YBCO film, and the corresponding curves for these dependences on graphics completely match. Figure 7 shows that in a moderately irradiated film ($S1$), the reactance X_s does not change

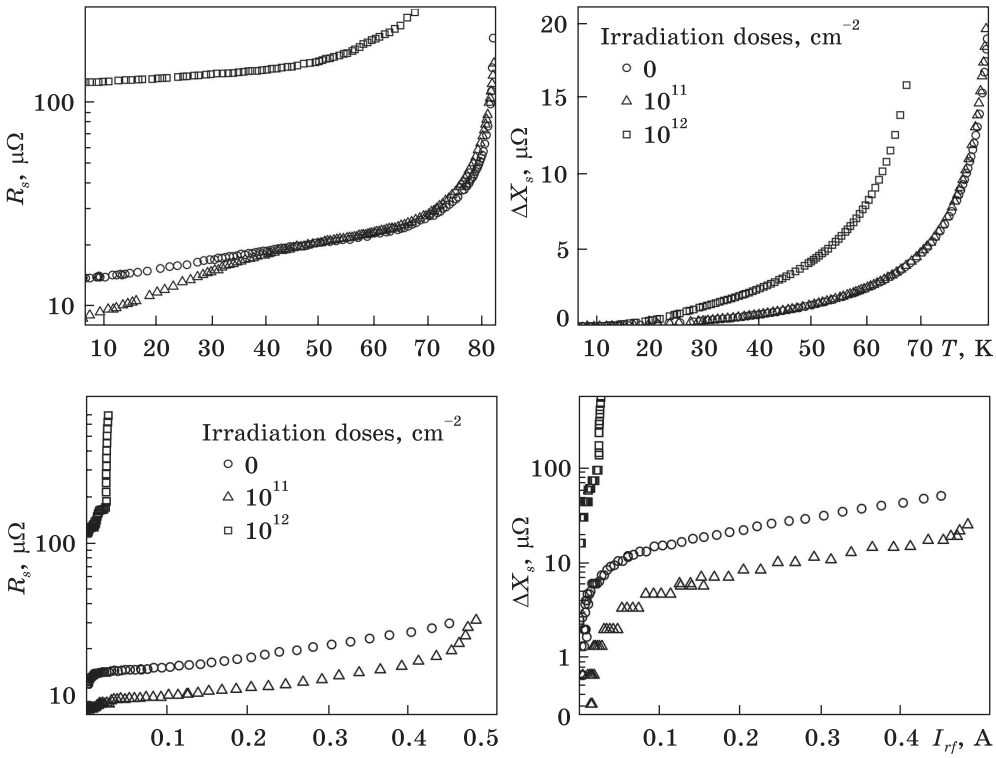

Fig. 7. Temperature dependences of surface resistance $R_s(T)$ and changes in reactance $\Delta X_s(T)$ for YBCO films irradiated with Au^{2+} ions with an energy of 3 MeV at different doses of irradiation: circle ○ (*S*0) — non-irradiated pure YBCO film; triangle △ (*S*1) — 10^{11} cm^{-2}; square □ (*S*2) — 10^{12} cm^{-2} [35]

Fig. 8. The same as in the previous figure but the dependences of the surface impedance on the microwave current amplitude at T = 4.2 K [35]

compared to that in a non-irradiated film (*S*0), and the surface resistance $R_s(T)$ is almost the same for both of these films at all temperatures, except the low-temperature region (T < 30 K), where the value of $R_s(T)$ for the film *S*1 is significantly smaller than for the film *S*0. On the other hand, as follows from the results presented in Fig. 7, at higher doses of irradiation (*S*2), there is a significant degradation of superconductivity compared to the original film (*S*0). The most interesting feature of the dependences Rs(T) and $\Delta X_s(T)$ presented in Fig. 7, there is a significant decrease in the surface resistance $R_s(T)$ at low temperatures (<30 K) for a moderately irradiated film (*S*1). The reactance of this film does not change compared to the initial film (*S*0) in the entire temperature range. This circumstance allows us to conclude that the described decrease of the surface resistance at low temperatures arises due to the enhancement of quasiparticle scattering by irradiation-induced structural defects and a corresponding increase

of the electron-momentum relaxation rate. As it is described in section 2 of this article, this should manifest itself at low temperatures, when electron–phonon scattering becomes insignificant, in a decrease of the real part of microwave conductivity, $\sigma_1(T, \omega)$, which is ensured by thermally excited quasiparticles in the Meissner state of the superconductor, and correspondingly the surface resistance $R_s(T, \omega)$. For heavily irradiated films ($S2$), the surface resistance and reactance are significantly higher than for the films $S0$ and $S1$. The latter indicates significant structural changes in $S2$ films and inhibition of superconductivity in these films at high doses of irradiation.

The influence of ion irradiation on the dependence of the surface impedance of the studied YBCO films on the microwave current amplitude is shown in Fig. 8. It can be seen that the nonlinear effects in the surface impedance (both the real and imaginary parts, $R_s(I_{RF})$ and $\Delta X_s(I_{RF})$) are noticeably weaker in the moderately irradiated film ($S1$) compared to the original film ($S0$), while for the strongly irradiated film ($S2$), these nonlinear effects become much larger. Insignificant quasi-linear growth of surface resistance and reactance with increasing microwave current amplitude, which is shown in Fig. 8, may be related to the existence of weak links in the film interior [37, 38].

In general, as it follows from the results presented in Fig. 7 and Fig. 8, ion irradiation with Au^{2+} ions with an energy of 3 MeV, carried out in moderate doses (curves $S1$), and favourably affects the microwave characteristics of the studied YBCO films. First, such radiation treatment significantly reduces the low-temperature surface resistance $R_s(T)$, and also improves the linearity of the microwave response due to the reduction of the dependences $R_s(I_{RF})$ and $\Delta X_s(I_{RF})$), as shown in Fig. 7 for moderate radiation dose ($S1$ curves for $Rs(I_{RF})$ and $\Delta X_s(I_{RF})$ dependences). Our explanation for an improvement of the linearity of microwave response in moderately irradiated YBCO films is described in the previous section 4 of this article.

6. Dissociation of Abrikosov Vortices and Nonlinearity of Microwave Response in Multiband Superconductors

6.1. Dissociation of Abrikosov Vortices in a Strong RF Field

In several theoretical works, it was argued that under certain conditions Abrikosov vortices in multiband superconductors can split and exist in the form of fractional vortices, formed separately in superfluid condensates of different electron bands [40–43]. Such vortices possess a fractional flux quantum, and these fractional vortices attract each other, trying to join into a composite vortex with the whole flux quantum $\phi_0 = h/(2e)$.

In this section, we explore the nonlinear ac dynamics of a composite vortex in a two-band superconductor settled in the pinning potential well

of columnar defect $U_p(r)$ and exerted to the action of RF Lorentz force. We consider the possibility of the composite vortex depinning as well as its dissociation into fractional components at high RF current amplitudes. For the pinning potential $U_p(r)$, the Lorentzian form was chosen, as it was suggested in several theoretical works [23, 27],

$$U_p(r) = -U_0 \frac{r_p^2}{r_p^2 + r^2}. \tag{26}$$

It was argued that fractional vortices from the same electron band repulse each other, whereas fractional vortices from different bands attract each other. This attraction is given by the potential [41, 43, 44]

$$V_{int}(r_{12,ij}) = \frac{\phi_1\phi_2}{8\pi^2\lambda^2}\left[K_0\left(\frac{|r_{12,ij}|}{\lambda}\right) + \ln(|r_{12,ij}|)\right], \quad \mathbf{r}_{12,ij} \equiv \mathbf{r}_{1,i} - \mathbf{r}_{2,j}, \tag{27}$$

where K_0 is the Macdonald function of the order zero. The attractive force between fractional vortices from different bands can be found as $F_{int}(r_{12,ij}) = \partial V_{int}(r_{12,ij})/\partial r_{12,ij}$ $(i \neq j)$.

We investigate vortex dynamics in a two-band superconductor, which arises under the RF Lorentz force action, by numerical solution of nonlinear dynamic equations, written for fractional vortices with reduced flux quanta $\phi_{1,2}$, and the interaction potential, $V_{int}(x_1 - x_2)$, given by Eq. (27) [45]. At low current densities, these fractional vortices constitute the composite vortex with a whole flux quantum ϕ_0, settled in the pinning potential well $U_p(r)$, given by Eq. (26). The corresponding coupled dynamic equations for oscillations of fractional vortices under the RF Lorentz force action can be written as follows

$$\begin{cases} \eta_1\dot{x}_1 + f_{p,1}(x_1(t)) + \dfrac{\phi_1\phi_2}{2\pi\mu_0\lambda^3}\,\mathrm{Re}\left[\dfrac{\lambda}{x_1 - x_2} - K_1\left(\dfrac{x_1 - x_2}{\lambda}\right)\right] = J_{ext}(t)\phi_1, \\ \eta_2\dot{x}_2 + f_{p,2}(x_2(t)) + \dfrac{\phi_1\phi_2}{2\pi\mu_0\lambda^3}\,\mathrm{Re}\left[\dfrac{\lambda}{x_2 - x_1} - K_1\left(\dfrac{x_2 - x_1}{\lambda}\right)\right] = J_{ext}(t)\phi_2. \end{cases} \tag{28}$$

Here, η_i is the viscosity coefficient (per unit length) for the fractional vortex formed in i-th band ($i = 1, 2$), $\eta_i = \phi_0^2/(2\pi\xi_i^2\rho_n)$, where ξ_i is the coherence length for the i-th band; $K_1(x)$ is the Macdonald function of the first order; $J_{ext}(t) = j_0\cos(\omega t)$ is the RF current density. Hereafter we consider the two-dimensional case $d \geq \lambda$ (d is the superconductor plate thickness) and disregard the thickness dependence of the current density as well as a possible vortex bending. $f_p(x_i)$ is the pinning force exerted on the fractional vortex (per unit length) within the pinning potential well (26).

Solution of the system of Eqs. (28) gives time-dependent coordinates, $x_j(t)$, which form in (x,t)-plane trajectories of motion for fractional vortices, moving under the RF Lorentz force action. These trajectories stick

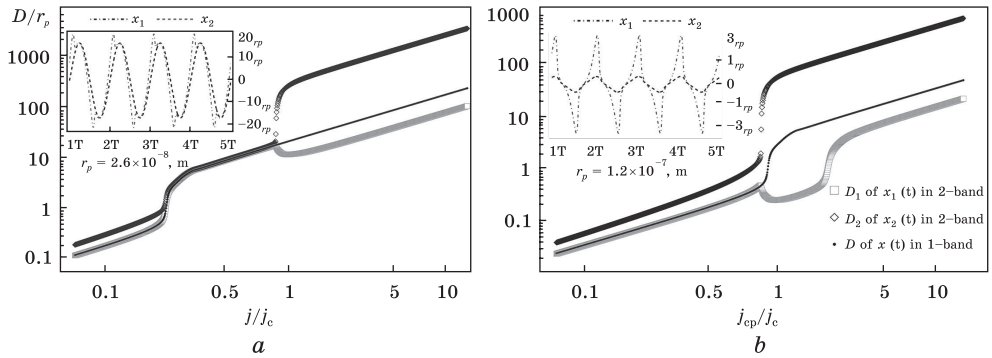

Fig. 9. Dependences of the maximal displacement $D(j_0)$ for $x_{1,2}(t)$ and $x(t)$ trajectories of fractional and composite vortices on the RF current amplitude j_0, obtained by numerical solution of Eqs. (28) for two different values r_p of the pinning potential well radius: $r_p = 2.6 \cdot 10^{-8}$ m (*a*) and $r_p = 1.26 \cdot 10^{-7}$ m (*b*) [45]

together at low alternating current amplitudes, and in this case, fractional vortices oscillate together, being coupled in a composite vortex. At high alternating current amplitudes, when j_0 exceeds some critical value j_c, the common trajectory for the composite vortex motion, $x(t)$, at definite moments during the period of oscillations splits into two different trajectories, $x_1(t)$ and $x_2(t)$, which resemble the separate dynamics of fractional vortices. Therefore, jc corresponds to the onset of the composite vortex dissociation under the RF Lorentz force action, which is different for fractional vortices from different bands. These split trajectories, $x_{1,2}(t)$, for fractional vortices, which arise at $j_0 > j_c$, are shown in insets to Fig. 9, while the main part of these figures demonstrates the amplitude of RF oscillations, $D(j_0, \omega)$, for oscillating fractional vortices and also for the composite vortex (*i.e.*, maximum of $x_{1,2}(t)$ and maximum of $x(t)$ as functions of RF current amplitude j_0). In Fig. 9, one can see steps on $D(j_0)$ dependences for maximal displacements of $x_{1,2}(t)$ and $x(t)$ trajectories.

The step on the $D(j_0)$ curve for $x(t)$ corresponds to the depinning of the composite vortex and arises at the current density amplitude denoted as j_p. On the other hand, the dissociation of the composite vortex into fractional components proceeds at the critical current density denoted as j_c. The split of trajectories $x_{1,2}(t)$ for fractional vortices, which arises at $j_0 > j_c$, is shown in insets to Fig. 9, *a*, *b*. The current density in Fig. 9 is normalized just by the jc value. The relation between jp and jc values depends on details of the pinning parameters, *i.e.* on the radius of the pinning potential well, as can be seen in Fig. 9.

The dynamic depinning and dissociation of composite vortices into fractional ones should manifest themselves in peculiarities of RF electrodynamic characteristics, such as the complex RF resistivity, as shown in the next subsection.

6.2. Nonlinear RF Vortex Response

In this subsection, we consider the nonlinear electrodynamic response of pinned composite vortices in a two-band superconductor driven by strong RF current action. Generally, the electric field induced by RF oscillations of fractional vortices, $x_{1,2}(t)$, can be written as follows

$$E(t) = n_{\phi}(\phi_1 \dot{x}_1 + \phi_2 \dot{x}_2). \tag{29}$$

One can represent this field in the form of Fourier series:

$$E(t) = \sum_n (E_{1,n}(\omega)\cos n\omega t + E_{2,n}(\omega)\sin n\omega t). \tag{30}$$

Then, the complex resistivity for each harmonic can be written in the following way:

$$\rho_n(\omega; j_0) = \rho_{1,n}(\omega; j_0) + i\rho_{2,n}(\omega; j_0) = \frac{E_{1,n}(\omega)}{j_0} + i\frac{E_{2,n}(\omega)}{j_0}. \tag{31}$$

The complex resistivity (31) reveals a strong nonlinear dependence on the RF current amplitude, j_0. This nonlinearity most distinctly manifests itself at critical current densities j_p and j_c, corresponding to the depinning and dissociation of the composite vortices, respectively. This type of nonlinearity is shown in Fig. 10 both for the real and imaginary parts of the resistivity at the 1st harmonic, $\rho_1(\omega;j_0)$.

Thus, from the obtained numerical solution of the nonlinear dynamic equations, which describe RF-current driven oscillations of Abrikosov vortices in the pinning potential well, formed by the columnar defect in a two-band superconductor, it follows that there is the possibility of fractional vortices formation in a two-band superconductor due to dissociation of composite Abrikosov's vortices with a whole flux quantum ϕ_0 under the sufficiently strong RF current action [45]. This dissociation takes place

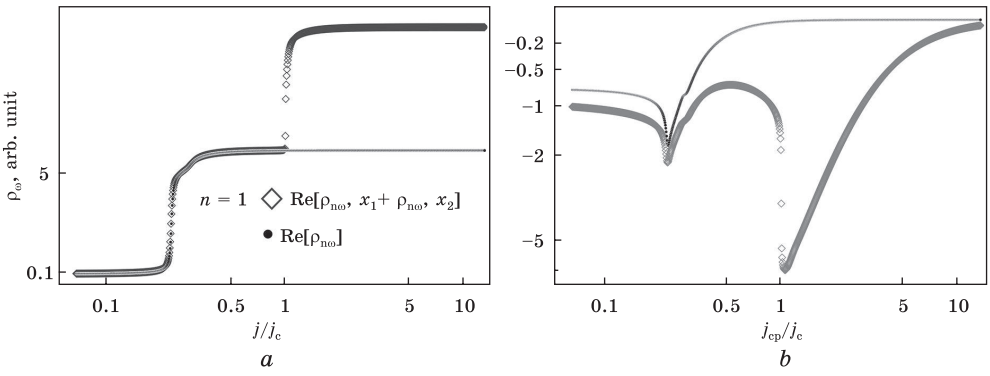

Fig. 10. Real (*a*) and imaginary (*b*) parts of the resistivity at the 1-st harmonic, $\rho_1(\omega)$, as functions of the RF current density amplitude j_0. The pinning potential and vortex trajectories $x_{1,2}(t)$ are that as in Fig. 9, *a*. Steps of the real part of $\rho_1(\omega; j_0)$ dependence on the RF current density amplitude j_0 correspond to depinning and dissociation of the composite vortices, respectively [45]

because of the different flux values $\phi_{1,2}$, related to fractional vortices from two different electron bands, and correspondingly — different values of the Lorentz forces acting on these vortices. In addition, the difference in viscosity coefficients, $\eta_{1,2}$, for fractional vortices supports this type of dynamic dissociation. The amplitude of the RF critical current density, j_c, causing dissociation of the composite vortex depends on the frequency, and it is different from the depinning critical current density, j_p. This type of composite vortex dissociation into the fractional vortices should be observable in RF experiments via specific peculiarities of the RF complex resistivity as well as in the emergence of specific peculiarities in the generation of higher harmonics. Generation of higher harmonics ($n = 2, 3, ...$) is a direct consequence of nonlinear response and the most pronounced features of this nonlinearity can be seen as peculiarities in the current dependences of $\rho_n(\omega; j_0)$, arising at $j_0 = j_p$ and $j_0 = j_c$.

7. Conclusion

We have elaborated the phenomenological model for microwave response in moderately anisotropic superconductors with artificial defect nanostructure, which consists of point-like and/or columnar defects with a nanosized cross-section. In the framework of this model, we argued that the formation of artificial defect nanostructure of this type could noticeably improve electrodynamic characteristics of a superconducting material like REBCO at microwave frequencies both in the Meissner and mixed states and in the nonlinear regime. Namely, we have demonstrated that the addition of 0*D* and 1*D* structural defects at not-too-high concentrations decreases the microwave surface resistance and enhances the nonlinearity threshold, thus increasing the range of the linear response.

We have carried out experimental studies of the effect of ion irradiation-induced structural point-like defects in HTS YBCO films on their microwave characteristics. These studies have revealed that irradiation of YBCO films with 3 MeV Au^{2+} ions at moderate doses of 10^{11} ions/cm^2 noticeably decreases the surface resistance of the film and increases its linearity at frequencies ≈1 GHz at low temperatures (<30 K). These experimental results agree well with the elaborated theoretical model described in this work.

In addition, we present theoretical results, which concern the new unusual mechanism of nonlinearity of RF response in multiband superconductors. This mechanism of nonlinearity is based on the possible dissociation of Abrikosov's vortices in multiband superconductors into fractional ones under the strong RF current action. We solved numerically the dynamic equation for vortex oscillations under the RF current action in a two-band superconductor containing columnar vortex pinning sites and found the vortex depinning and dissociation threshold RF current amplitudes. We

have also calculated the RF complex resistivity and emergence of specific peculiarities in the generation of its harmonics. Thus, we argue that RF measurements performed on multiband superconductors should reveal new features of the vortex matter in multiband superconductors.

Acknowledgement. This work was partly supported by the National Research Foundation of Ukraine through the project 2020.02/0408.

REFERENCES

1. B. Maiorov, S.A. Baily, H. Zhou, O. Ugurlu, J.A. Kennison, P.C. Dowden, T.G. Holesinger, S.R. Foltyn, and L. Civale, *Nature Mater.*, **8**: 398 (2009). https://doi.org/10.1038/nmat2408
2. T.G. Holesinger, M.D. Feldmann, B. Maiorov, L. Civale, J.A. Kennison, Y.J. Coulter, P.D. Dowden, J.F. Baca, P.H. Tobash, E.D. Bauer, and K.R. Marken, *Materials*, **4**, No. 11: 2042 (2011). https://doi.org/10.3390/ma4112042
3. S.H. Wee, Y.L. Zuev, C. Cantoni, and A. Goyal, *Sci. Rep.*, **3**: 2310 (2013). https://doi.org/10.1038/srep02310
4. T. Horide, K. Otsubo, R. Kita, N. Matsukida, M. Ishimaru, S. Awaji, and K. Matsumoto, *Supercond. Sci. Technol.*, **30**, No. 7: 074009 (2017). https://doi.org/10.1088/1361-6668/aa70d3
5. V.L. Svetchnikov, V.S. Flis, A.A. Kalenyuk, A. L.Kasatkin, A.I. Rebikov, V.O. Moskaliuk, C.G. Tretiatchenko, and V.M. Pan, *J. Phys.: Conf. Ser.*, **234**: 012041 (2010). https://iopscience.iop.org/article/10.1088/17426596/234/1/012041
6. V.I. Matsui ,V.S. Flis, V.O. Moskaliuk, A.L. Kasatkin, N.A. Skoryk, V.L. Svechnikov, *J. Nanosci. Nanoeng.*, **1**, No. 2: 38 (2015). http://files.aiscience.org/journal/article/html/70270011.html
7. L. Civale, *Supercond. Sci. Technol.*, **10**, No. 7A: A11 (1997). https://iopscience.iop.org/article/10.1088/0953-2048/10/7A/003
8. R. Biswal, J. John, P. Mallick, B.N. Dash, P.K. Kulriya, D.K. Avasthi, D. Kanjilal, D. Behera, T. Mohanty, P. Raychaudhuri, and N.C. Mishra, *J. Appl. Phys.*, **106**, No. 5: 053912 (2009). https://doi.org/10.1063/1.3212537
9. F. Massee, P.O. Sprau, Y.-L. Wang, J.C.S. Davis, G. Ghigo, G. Gu, W.-K. Kwok, *Sci. Adv.*, **1**, No. 4: e1500033 (2015). https://www.science.org/doi/10.1126/sciadv.1500033
10. J. Wosik, L.-M. Xie, J. Mazierska, and R. Grabovickic, *Appl. Phys. Lett.*, **75**, No. 12: 1781 (1999). https://doi.org/10.1063/1.124818
11. R. Gerbaldo, G. Ghigo, L. Gozzelino, F. Laviano, A. Amato , A. Rovelli, and R. Cherubini, *AIP Conf. Proc.*, **1530**, No. 1: 95 (2013). https://doi.org/10.1063/1.4812910
12. R. Woerdenweber, P. Lahl, and J. Einfeld, *IEEE Trans. Appl. Supercond.*, **11**, No. 1: 2812 (2001). https://ieeexplore.ieee.org/document/919648
13. S. Ohshima, N. Takanashi, A. Saito, K. Nakajima, and T. Nagayama, *IEEE Trans. Appl. Supercond.*, **28**, No. 4: 1 (2018). https://ieeexplore.ieee.org/document/8299455
14. S. Sato, T. Honma, S. Takahashi, K. Sato, M. Watanabe, K. Ichikawa, K. Takeda, K. Nakagawa, A. Saito, and S. Ohshima, *IEEE Trans. Appl. Supercond.*, **23**, No. 3:

7200404 (2013).
https://ieeexplore.ieee.org/document/6380552
15. P.A. Borisenko, A.O. Pokusinskii, and A.L. Kasatkin, *Ukr. J. Phys.*, **64**, No. 10: 969 (2019).
https://doi.org/10.15407/ujpe64.10.969
16. A. Pokusinskyi, A. Kasatkin, S. Futimsky, O. Kalenyuk, O. Boliasova, and A. Shapovalov, *J. Appl. Phys.*, **132**, No. 23: 233904 (2022).
https://doi.org/10.1063/5.0121793
17. A.L. Kasatkin, A.O. Pokusinskyi, O.O. Boliasova, V.P. Tsvitkovskyi, and A.P. Shapovalov, *Low Temp. Phys.*, **49**, No. 9: 1009 (2023).
https://doi.org/10.1063/10.0020592
18. A. Hosseini, R. Harris, S. Kamal, P. Dosanjh, J. Preston, R. Liang, W.N. Hardy, and D.A. Bonn, *Phys. Rev. B*, **60**, No. 2: 1349 (1999).
https://doi.org/10.1103/PhysRevB.60.1349
19. P.J. Hirschfeld and N. Goldenfeld, *Phys. Rev. B*, **48**, No. 6: 4219 (1993).
https://doi.org/10.1103/PhysRevB.48.4219
20. R. Prozorov and R. Giannetta, *Supercond. Sci. Technol.*, **19**, No. 8: R41 (2006).
https://iopscience.iop.org/article/10.1088/0953-2048/19/8/R01
21. M. Golosovsky, M. Tsindlekht, and D. Davidov, *Supercond. Sci. Technol.*, **9**, No. 1: 1 (1996).
https://iopscience.iop.org/article/10.1088/0953-2048/9/1/001
22. E.H. Brandt, *Phys. Rev. Lett.*, **69**, No. 7: 1105 (1992).
https://doi.org/10.1103/PhysRevLett.69.1105
23. E.H. Brandt, *Rep. Prog. Phys.*, **58**, No. 11: 1465 (1995).
https://doi.org/10.1088/0034-4885/58/11/003
24. M.W. Coffey and J.R. Clem, *Phys. Rev. Lett.*, **67**, No. 3: 386 (1991).
https://doi.org/10.1103/PhysRevLett.67.386
25. M.W. Coffey and J.R. Clem, *Phys. Rev. B*, **46**, No. 18: 11757 (1992).
https://doi.org/10.1103/PhysRevB.46.11757
26. J.I. Gittleman and B. Rosenblum, *Phys. Rev. Lett.*, **16**, No. 17: 734 (1966).
https://doi.org/10.1103/PhysRevLett.16.734
27. G. Blatter, M.V. Feigel'man, V.B. Geshkenbein, A.I. Larkin, and V.M. Vinokur, *Rev. Mod. Phys.*, **66**, No. 4: 1125 (1994).
https://doi.org/10.1103/RevModPhys.66.1125
28. A.V. Velichko, M.J. Lancaster, and A. Porch, *Supercond. Sci. Technol.*, **18**, No. 3: R24 (2005).
https://doi.org/10.1088/0953-2048/18/3/R02
29. M.A. Hein, R.G. Humphreys, P.J. Hirst, S.H. Park, and D.E. Oates, *J. Supercond.*, **16**: 895 (2003).
https://doi.org/10.1023/A:1026219405360
30. S.M. Anlage, W. Hu, C.P. Vlahacos, D. Steinhauer, B.J. Feenstra, S.K. Dutta, A. Thanawalla, and F.C. Wellstood, *J. Supercond.*, **12**: 353 (1999).
https://doi.org/10.1023/A:1007753316152
31. M.I. Tsindlekht, E.B. Sonin, M.A. Golosovsky, and D. Davidov, *Phys. Rev. B*, **61**, No. 2: 1596 (2000).
https://doi.org/10.1103/PhysRevB.61.1596
32. A. Gurevich and G. Ciovati, *Phys. Rev. B*, **77**, No. 10: 104501 (2008).
https://doi.org/10.1103/PhysRevB.77.104501
33. J.R. Powell, A. Porch, A.P. Kharel, M.J. Lancaster, R.G. Humphreys, F. Wellhofer, and C.E. Gough, *J. Appl. Phys.*, **86**, No. 4: 2137 (1999).
https://doi.org/10.1063/1.371021

34. V.S. Flis, A.A. Kalenyuk, A.L. Kasatkin, V.O. Moskalyuk, A.I. Rebikov, V.L. Svechnikov, K.G. Tret'yachenko, and V.M. Pan, *Low Temp. Phys.*, **36**, No. 1: 59 (2010). https://doi.org/10.1063/1.3292938
35. A.A. Kalenyuk, A.L. Kasatkin, S.I. Futimsky, A.O. Pokusinskiy, T.A. Prikhna, A.P. Shapovalov, V.E. Shaternik, and Sh. Akhmadaliev, *Supercond. Sci. Technol.*, **36**, No. 3: 035009 (2023). https://doi.org/10.1088/1361-6668/acb110
36. M. Leroux, K.J. Kihlstrom, S. Holleis, M.W. Rupich, S. Sathyamurthy, S. Fleshler, H.P. Sheng, D.J. Miller, S. Eley, L. Civale, A. Kayani, P.M. Niraula, U. Welp, and W.-K. Kwok, *Appl. Phys. Lett.*, **107**, No. 19: 192601 (2015). https://doi.org/10.1063/1.4935335
37. H. Matsui, H. Ogiso, H. Yamasaki, T. Kumagai, M. Sohma, I. Yamaguchi, and T. Manabe, *Appl. Phys. Lett.*, **101**, No. 23: 232601 (2012). https://doi.org/10.1063/1.4769836
38. J. Halbritter, *J. Appl. Phys.*, **68**, No. 12: 6315 (1990). https://doi.org/10.1063/1.346875
39. J. Kermorvant, C.J. van der Beek, J.-C. Mage, B. Marcilhac, Y. Lemaotre, J. Briatico, R. Bernard, and J. Villegas, *J. Appl. Phys.*, **106**, No. 2: 023912 (2009). https://doi.org/10.1063/1.3079520
40. E. Babaev, *Phys. Rev. Lett.*, **89**, No. 6: 067001 (2002). https://doi.org/10.1103/PhysRevLett.89.067001
41. M.A. Silaev, *Phys. Rev. B*, **83**, No. 14: 144519 (2011). https://doi.org/10.1103/PhysRevB.83.144519
42. Y. Tanaka, *Supercond. Sci. Technol.*, **28**, No. 3: 034002 (2015). https://doi.org/10.1088/0953-2048/28/3/034002
43. S.-Z. Lin, *J. Phys.: Condens. Matter*, **26**, No. 49: 493202 (2014). https://doi.org/10.1088/0953-8984/26/49/493202
44. S.-Z. Lin and L.N. Bulaevskii, *Phys. Rev. Lett.*, **110**, No. 8: 087003 (2013). https://doi.org/10.1103/PhysRevLett.110.087003
45. A.O. Pokusinskyi and A.L. Kasatkin, *Low Temp. Phys.*, **50**, No. 2, 111 (2024). https://doi.org/10.1063/10.0024321

Received 30.11.2023
Final version 01.12.2023

О.Л. Касаткін[1,2], *О.А. Каленюк*[1,3],
А.О. Покусінський[4], *С.І. Футимський*[1], *А.П. Шаповалов*[1,3]
[1] Інститут металофізики ім. Г.В. Курдюмова НАН України,
бульв. Академіка Вернадського, 36, 03142 Київ, Україна
[2] Інститут надтвердих матеріалів ім. В.М. Бакуля НАН України,
вул. Автозаводська, 2, 07074 Київ, Україна
[3] Київський академічний університет,
бульв. Академіка Вернадського, 36, 03142 Київ, Україна
[4] Факультет радіофізики, електроніки та комп'ютерних систем,
Київський національний університет імені Тараса Шевченка,
просп. Академіка Глушкова, 4г, 03187 Київ, Україна

ВИСОКОЧАСТОТНА ЕЛЕКТРОДИНАМІКА НАНОСТРУКТУРОВАНИХ БАГАТОЗОННИХ НАДПРОВІДНИКІВ

На основі феноменологічної теорії мікрохвильового відгуку надпровідників II роду проаналізовано вплив штучно створеної наноструктури 0*D*- і 1*D*-структурних дефектів, утвореної імплантованими діелектричними наночастинками або радіацій-

ними дефектами, на мікрохвильові властивості плівок високотемпературного надпровідника (ВТНП). Поверхневий опір розраховано як для мейсснерівського, так і для змішаного станів для такого типу наноструктурованої плівки надпровідника II роду. Також теоретично досліджено появу нелінійного відгуку, спричиненого проникненням вихорів, індукованих мікрохвильовим полем, у внутрішню частину плівки через її краї. Одержані результати свідчать про те, що штучна дефектна наноструктура всередині може значно поліпшити її мікрохвильові характеристики як у мейсснерівському, так і в змішаному станах, а також збільшити діапазон лінійного мікрохвильового відгуку. Наведено також результати експериментальних досліджень мікрохвильових властивостей плівок ВТНП зі штучною дефектною наноструктурою, сформованою опроміненням важкими іонами. Помітне зниження поверхневого опору та збільшення діапазону лінійного відгуку за низьких температур спостерігалося для помірно опроміненої ВТНП-плівки $YBa_2Cu_3O_{7-x}$ (YBCO) під впливом опромінення іонами Au^{2+} з енергією у 3 МеВ із дозою у 10^{11} см$^{-2}$. Ці результати узгоджуються з феноменологічною теорією мікрохвильового відгуку наноструктурованих надпровідників, зазначеною вище. Представлено також теоретичну модель нового незвичайного механізму нелінійного радіочастотного відгуку в багатозонних надпровідниках. Це — механізм нелінійності, заснований на можливій дисоціації вихорів Абрикосова у багатозонних надпровідниках на фракційні складові під дією сильного високочастотного струму. Розраховано питомий ВЧ-комплексний опір у двозонних надпровідниках і обґрунтовано появу специфічних особливостей за критичних значень густини струму, що відповідають депінінґу та дисоціації вихорів.

Ключові слова: високотемпературний надпровідник (ВТНП), точковоподібні дефекти, стовпчасті дефекти, іонне опромінення, мікрохвильове поле, поверхневий імпеданс, нелінійний відгук.